5.1. Cell-line Studies

Various *in vitro* cell line studies were carried out for further screening of prepared immune-nanoparticles to achieve maximum chemotherapeutic drug uptake inside the cells.(1,2)

5.1.1. In Vitro Cytotoxicity Assay (MTT Assay)(3–5)

MTT Assay is a colorimetric assay that measures the reduction of yellow 3-(4,5-dimethythiazol- 2-yl)-2,5-diphenyl tetrazolium bromide (MTT) by mitochondrial succinate dehydrogenase. The MTT enters the cells and passes into the mitochondria where it is reduced to an insoluble, coloured (dark purple) formazan product. The cells are then solubilised with an organic solvent (eg. isopropanol) and the released, solubilised formazan reagent is measured spectrophotometrically. Since reduction of MTT can only occur in metabolically active cells the level of activity is a measure of the viability of the cells. Tetrazolium dye reduction is dependent on NAD(P)H dependent oxidoreductase enzymes largely in the cytosolic compartment of the cell. Therefore, reduction of MTT and other tetrazolium dyes increases with cellular metabolic activity due to elevated NAD(P)H flux. Resting cells such as thymocytes and splenocytes that are viable but metabolically quiet reduce very little MTT. In contrast, rapidly dividing cells exhibit high rates of MTT reduction. It is important to keep in mind that assay conditions can alter metabolic activity and thus tetrazolium dye reduction without affecting cell viability and that different tetrazolium dyes will give different results depending on whether they are reduced intracellularly (MTT, MTS) or extracellularly (6–9).

The cytotoxicity of immune-nanoparticles were determined using 3-(4, 5-dimethylthiazole-2-yl)- 2,5-diphenyl tetrazolium bromide (MTT; Himedia, India) assays. A549 cells were seeded onto 96-well plates at a density of 5×10^3 cells/well. After 24 h, cells were treated separately with Docetaxel, Docetaxel Nanoparticles and Cetuximab conjugated Docetaxel Nanoparticles in DMEM media containing 10% FBS and antibiotics (4).

In all wells, after 6 hr transfection media was replaced by fresh DMEM containing 10% of FBS and antibiotics. The cells were incubated for 48 hr, and then 20 µL of 5 mg/mL MTT solution was added to each well. After incubating for 4 hr with MTT solution, the culture medium was removed and 200 µL of a dimethyl sulfoxide was added. The reduction of viable cells was measured by calorimetry at 570 nm wavelength using an enzyme-linked immunosorbent assay (ELISA) plate reader (Bio-Rad, USA). Cell viability of each group was expressed as a relative percentage to that of control cells (9,8).

5.1.2 Confocal microscopy(10–14)

For several years, two advanced techniques, confocal laser scanning microscopy (CLSM) and flow cytometry, in particular fluorescence-activated cell sorting (FACS) have been used more and more to study the cellular uptake of targeted drug delivery systems.(15)(16) These techniques provide new potential to localize carriers in cells and quantify the amount of nanoparticulate formulation uptake, leading to essential information on the interaction between the formulation and the target cell. A better understanding of the underlying mechanism behavior of nanoparticulate formulation in biological systems is essential when adapting the nanoparticulate system in order to improve carrier effectiveness. (17–19)

Confocal microscopic (CSLM) analysis was carried out to know the presence of NP within the cells. The A549 cells were incubated on a confocal dish for 24 h, followed by fluorescent dye (6- Coumarin)-loaded Cetuximab conjugated Docetaxel Nanoparticles was treated to the cell line and allowed for 60 min. The cells were washed with PBS buffer and fixed with 4% paraformaldehyde (PFA) for 20 min. The cells were then stained with 4',6-diamidino-2-phenylindole (DAPI) for additional 15 min and subsequently, cells were washed, mounted and sealed with glycerine. The cells were observed under FV1000 confocal laser scanning microscope (Olympus, Japan) (20–22).

Imaging was carried out in A549 cells using three formulations, i.e. Cetuximab, Docetaxel Nanoparticles and Cetuximab conjugated Docetaxel Nanoparticles. $5x10^4$ cells were seeded onto confocal microscopic petridish with glass cover slip (Nunc, India). After 24 hr cells were transfected with 6-coumarin at 100 nM concentration. Soon after transfection imaging was started. Furthermore, the lateral Z-stack images were constructed during imaging from the middle zone of the cells (23–25).

5.1.3 Cellular uptake by flow cytometer analysis (4,26–28)

For cellular uptake studies, Flow cytometry was utilized for quantitative cell uptake to determine the mean fluorescent intensity while qualitative intracellular accumulation was determined using confocal microscopy (1,29,30).

In principle, flow cytometry can be combined with nearly any staining procedure, assay or biotechnological process. Whenever fluorescence is introduced into a microorganism or a cell it can be exploited in flow cytometry for assessing information about the specimen. To a low

extent the technology is applied for other objects than microorganisms and cells.(4,17,31) But with the combination of fluidics and laser triggered fluorescence detection it is the ideal tool to detect NPs in cells. Subtle changes in scattering and emission of a cell can be observed which are directly linked to the cellular uptake of fluorescing particles (32,33).

In flow cytometry, a fluidics system is coupled with the detection of fluorescence and of light scattering in small and wide angle position. For this application the objects of interest must be prepared as a diluted dispersion commonly not exceeding a concentration of several thousand objects per µl. In the machine, a sample stream is injected into the core of a flowing stream of so called sheath liquid (water or physiological buffer) and a laminar flow is established. The two streams do not mix and the sample flow is surrounded by a layer of sheath liquid flow in a concentric setup. This is termed hydrodynamic focusing. This stream of two concentric layers is directed through the measurement chamber, a narrow glass capillary. In the measurement chamber, the sample stream is hit orthogonally by a laser beam. It is important to note that the objects, e.g. cells, pass this laser beam single-filed. Placed behind an array of filters and mirrors, several detectors successively detect the properties of each cell passing the laser beam. This includes fluorescence signals but also of wide angle (sideward scatter, SSC) and small angle (forward scatter, FSC) scattering. Flow cytometers thus allow for the rapid measuring of individual objects in dispersion. Another obvious advantage is the short exposure of each object to the laser (µs scale), unlike e.g. in microscopy where exposure lasts seconds to minutes.(18,34) Extremely light sensitive objects can be analyzed by flow cytometry. Within one second, several thousand objects can be measured separately and their number per volume can be counted. But only when one object passes through the beam of the reference laser, data acquisition is triggered. In this instant, a digital event is created and the acquired data from every active channel is assigned to this event i.e. assigned to this particular object. Each event now represents a comprehensive data set, including fluorescence intensities in various channels and scattering intensities at two fixed positions (small and large angle i.e. FSC and SSC). This collected raw data consists of up to hundred thousands of events which represent background (e.g. pieces of cell debris) and wanted objects (cells) alike. (35) Before final data interpretation the signals must be sorted from the background events. Fluorescence, granularity (SSC) or the presumable size (FSC or SSC) are features which can be applied to identify the wanted objects. Commonly a threshold condition is set on one of the detection channels so that unwanted signals are excluded

from detection. In nearly every system a 488 nm laser is present as standard reference, but often additional lasers (e.g. 640 nm, 561 nm, 375 nm) are available (27).

The A549 cells were seeded at a density of $2X10^5$ cells/6-well plate and allowed to attach for 24 h. The cells were exposed to (6-Coumarin)- cetuximab conjugated Docetaxel nanoparticles and incubated for 2 h. The cells were washed twice with PBS, trypsinized, collected and re-suspended in PBS. The amount of cellular uptake of Docetaxel was confirmed by flow cytometry (36,37).

5.1.4 Apoptosis study using FACS

The A549 were seeded at a density of $2X10^5$ cells/6-well plate and allowed to attach for 24 h. The cells were treated with free Docetaxel, Docetaxel Nanoparticles and Cetuximab conjugated Docetaxel Nanoparticles and incubated for 24 h at 37 °C in a standard incubator. A control was maintained as untreated cells. After the incubation period, cells were trypsinized with 0.025% trypsin solution, harvested, and resuspended in a 200 ml of binding buffer. Immediately, 5 ml of annexin V-FITC and 8 ml of propidium iodide (PI) was added and gently votexed and kept aside for 15 min. The proportions of apoptotic or stained cells were observed by flow cytometer (38,39).

5.1.5 Cell cycle analysis by flow cytometry

A549 cells were seeded at a density of $2X10^5$ cells/6-well plate and allowed to attach for 24 h. The cells were treated with free ocetaxel, Docetaxel Nanoparticles and Cetuximab conjugated Docetaxel Nanoparticles and incubated for 24 h at 37 °C in a standard incubator. The cells were trypsinized, harvested, and centrifuged using a microcentrifuge at 1500 rpm for 4 min. The cell pellets were washed twice with PBS buffer and fixed in 75% ethanol solution at 4 °C. Cells were centrifuged, washed twice, and resuspended in PBS containing 5 mg/ml PI and 50 mg/ml deoxyribonuclease-free ribonuclease A. This suspension was incubated in dark atmosphere for 25 min and then cell cycle patterns were analyzed using flow cytometry (38).

5.2 Results and Discussion

5.2.1 *In Vitro* Cytotoxicity Assay (MTT Assay)

Polymeric nanoparticles fabricated from PLGA have been found to be effective for the delivery of both low molecular and macromolecular therapeutics as a ligand. Therapeutic efficiency of drug loaded nanoparticles would depend on nanoparticle uptake, their intracellular distribution, and more importantly on the dose of the drug that is released from the internalized nanoparticles inside the cell. To investigate the therapeutic efficiency of the formulations, A549 cells were treated with Docetaxel, Docetaxel Nanoparticles and Cetuximab conjugated Docetaxel Nanoparticles at different concentrations, and cell proliferation was measured by a standard MTT colorimetric assay. Results are shown in Table 5.1 and In vitro cytotoxicity analysis of Docetaxel, Docetaxel NP and Cetuximab conjugated Docetaxel Nanoparticles on A549 Cell lines at different time graphically described in Figure 5.2.

Table 5.1 Viability of A549 Cells on 24 h Exposure

Docetaxel (µg)		% Cell Viability			
	Exposure	PBS	Docetaxel Free Drug	Docetaxel Nanoparticles	Cetuximab conjugated Docetaxel Nanoparticles
0.0025	24 h	100.01 ± 3.15	95.85 ± 3.40	95.25 ± 3.54	95.57 ± 5.54
0.025		98.21 ± 4.54	92.36 ± 5.62	89.41 ± 3.92	81.14 ± 4.31
0.25		97.42 ± 5.36	70.22 ± 3.68	68.52 ± 2.93	59.18 ± 3.11
2.5		97.35 ± 2.48	52.78 ± 4.21	50.64 ± 3.87	37.27 ± 4.24
25		96.61 ± 4.25	38.98 ± 3.31	35.74 ± 4.55	15.64 ± 5.45
0.0025	48 h	103.21 ± 3.41	92.58 ± 3.51	89.51 ± 3.54	83.35 ± 5.62
0.025		100.25 ± 4.61	84.65 ± 5.67	79.35 ± 3.91	70.68 ± 4.25
0.25		95.85 ± 5.54	70.45 ± 3.74	60.38 ± 2.97	52.28 ± 3.54
2.5		98.24 ± 2.33	51.62 ± 4.58	38.58 ± 3.85	22.49 ± 4.84
25		92.67 ± 4.84	30.36 ± 3.81	22.52 ± 4.52	17.29 ± 5.61
0.0025	72 h	100.27 ± 3.71	91.28 ± 3.65	89.57 ± 3.54	84.34 ± 5.31
0.025		104.14 ± 4.82	80.57 ± 5.14	72.22 ± 3.94	67.16 ± 4.57
0.25		99.87 ± 5.93	63.67 ± 3.18	47.27 ± 2.87	45.54 ± 3.56
2.5		98.95 ± 2.54	44.94 ± 4.51	28.64 ± 3.81	23.66 ± 4.28
25		95.68 ± 4.67	35.18 ± 3.92	21.98 ± 4.54	13.47 ± 5.49

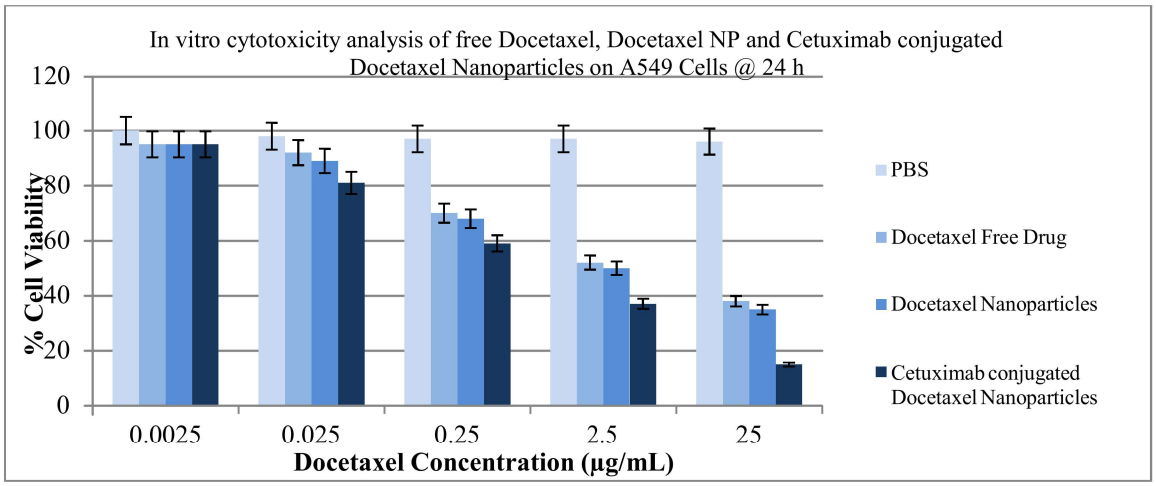

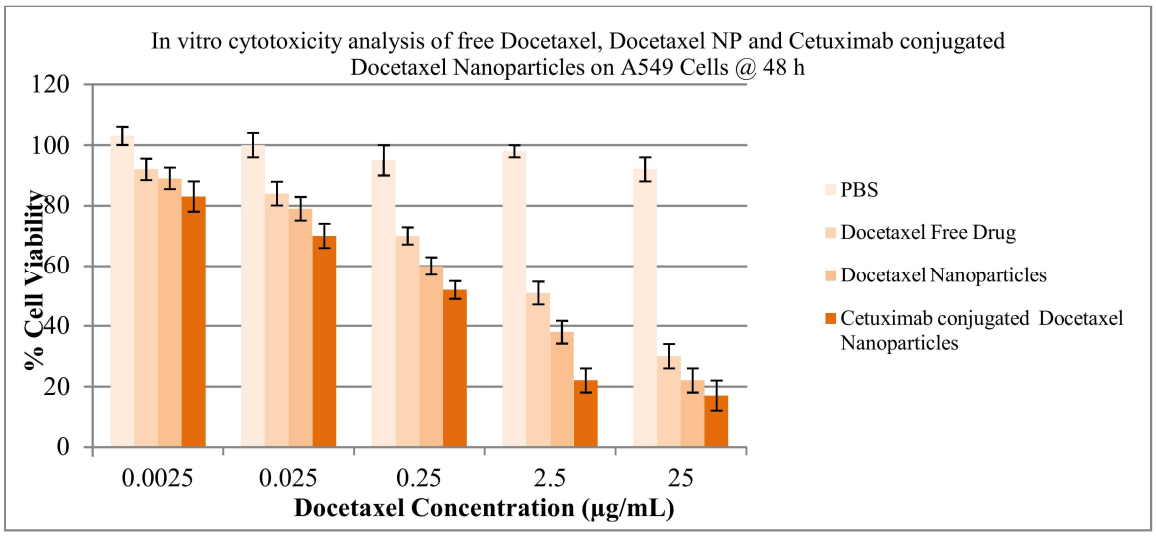

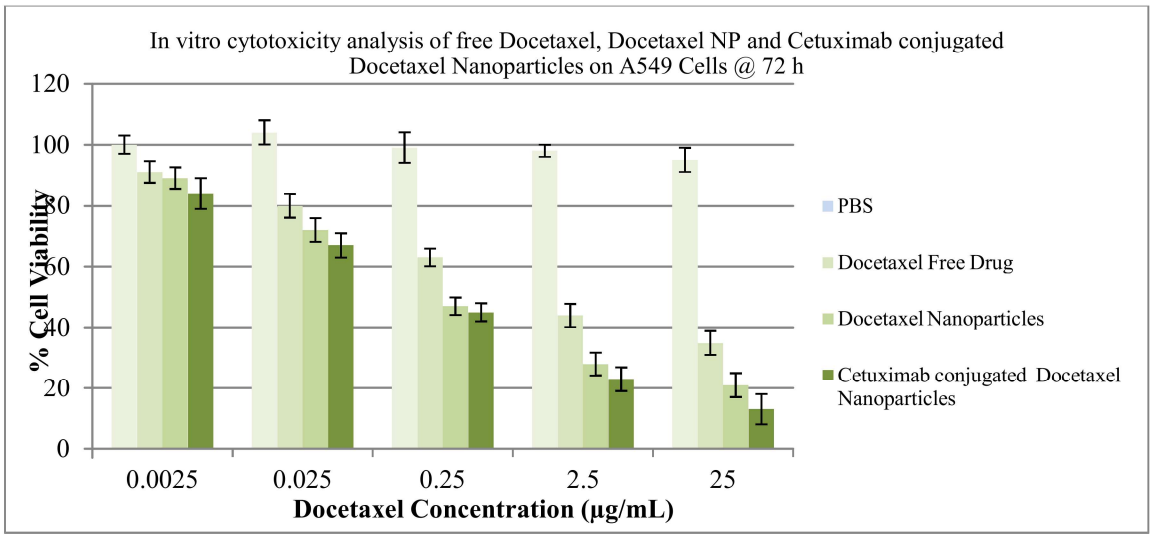

Figure 5.2 In vitro cytotoxicity analysis of Docetaxel, Docetaxel NP and Cetuximab conjugated Docetaxel Nanoparticles on A549 Cell lines at different time

In vitro cytotoxicity studies demonstrated that Cetuximab conjugated Docetaxel nanoparticles showed higher antiproliferative activity than unconjugated Docetaxel loaded nanoparticles and Docetaxel. Even at very low dose, targeted therapy was much more effective than Docetaxel loaded nanoparticles and Docetaxel. (40)

Cell inhibition effect of individual drug and antibody conjugated on A549 cells were evaluated by MTT assay. It can be seen that, Docetaxel, Docetaxel nanoparticles, and Cetuximab conjugated Docetaxel nanoparticles exhibited a time-dependent and dose-dependent cytotoxicity on both the cell lines tested. Although Docetaxel is a strong antimitotic cancer drug yet it cannot inhibit the cell proliferation completely. Similarly Docetaxel NP did not result in superior effect. On the other hand, Cetuximab conjugated to the Docetaxel NPs significantly reduced cell proliferation and increased the therapeutic efficiency of complex by suppressing the multidrug resistance phenomenon and exhibited a clear synergistic effect (**Figure 5.2**).

After 24 h incubation, as depicted in Fig. 6(a), the cell viability decreased to about 59.22, 47.12 and 38.45% for Cetuximab conjugated Docetaxel nanoparticles at 0.05, 0.5 and 5.0 g/ml drug concentrations respectively, corresponding to an increase in cytotoxicity of 25% compared with that of free drug. After 48 h incubation, portrayed in Fig. 6(b), the cytotoxicity increased to about 41.34, 35.12 and 25.31% for the DTX-CH-NP3 and 65.88, 58.98 and 48.87% for the free drug, respectively. The more marked inhibition of cell growth was obtained for longer incubation period (72 h). The strongest cytotoxic effect was achieved with nanoparticles at 5.0 g/ml drug concentration.

This results in the substantial reduction in the IC50 value of Docetaxel when used on synergistic combinations. The IC50 value of Docetaxel NP was 1.1 mg/ml, 0.32 mg/ml, 0.098 mg/ml after 24, 48, and 72 hours incubation, whereas Cetuximab conjugated Docetaxel NPs exhibited 0.18 mg/ml, 0.059 mg/ml, 0.012 mg/ml for respective incubation time in A549 cells. The superior antiproliferative effect of Cetuximab conjugated Docetaxel NPs was attributed to higher intracellular drug level and greater uptake efficiency which could be due to the anti EGFR effect of Cetuximab mAb .

5.2.2 Confocal microscopy observation

Confocal microscopy was employed to characterize the cellular internalization of Cetuximab conjugated Docetaxel nanoparticles in A549 cells. The nucleus was stained with DAPI. As shown in **Figure 5.3**, a strong red fluorescence was observed in the cytoplasmic region after incubation of NP for 60 min. In the merged image, clear red fluorescence in the peripheral cytoplasm and blue stained nucleus was observed indicating that NP was internalized via endocytosis mechanism. This would allow it to target directly in the microtubules which is present in the cytoplasmic region (18).

Additionally, results obtained in our studies results showing enhanced efficacy of docetaxel in presence of Cetuximab warrant the efficient specific tagetting to EGFR receptor.

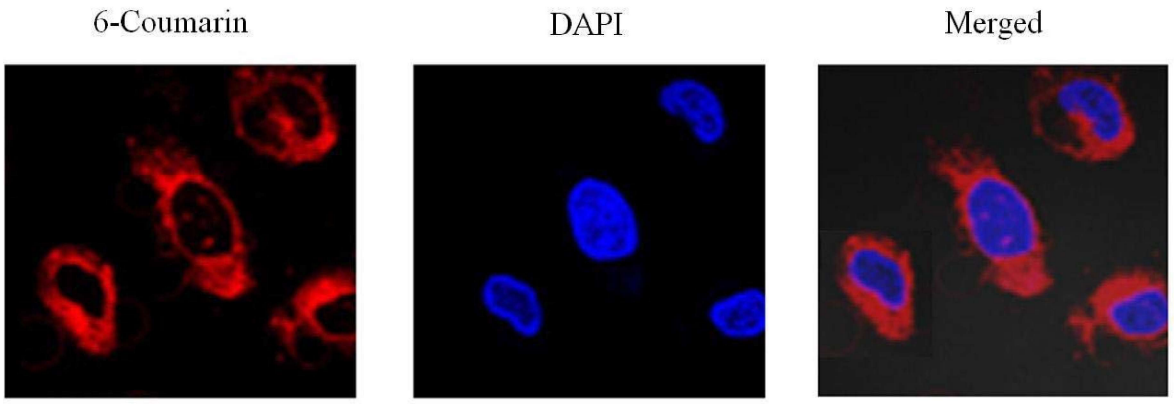

Figure 5.3 Confocal microscope images of intracellular distribution of Cetuximab conjugated Docetaxel nanoparticles in A549 cells after incubation for 1 h. Cell nuclei was stained with DAPI (blue) and endosomes/lysosomes were stained by cy.5 (red).

5.2.3 Cellular uptake by flow cytometry

Flow cytometer analysis was carried out to further confirm the cellular uptake of cetuximab conjugated Docetaxel nanoparticles in A549 cells. As is seen, remarkable increase in the fluorescence intensity was observed following 30 min incubation (Figure 5.4). Moreover, cellular uptake of NP further increased when the incubation time is increased to 60 min. The observation is consistent with the cytotoxicity assay which depicted a time-dependent cell inhibition effect. Both the confocal and flow cytometry analysis indicates that NP systems can

effectively deliver the active ingredient into the cell cytoplasm that will improve the therapeutic efficacy in tumors (18,20,41).

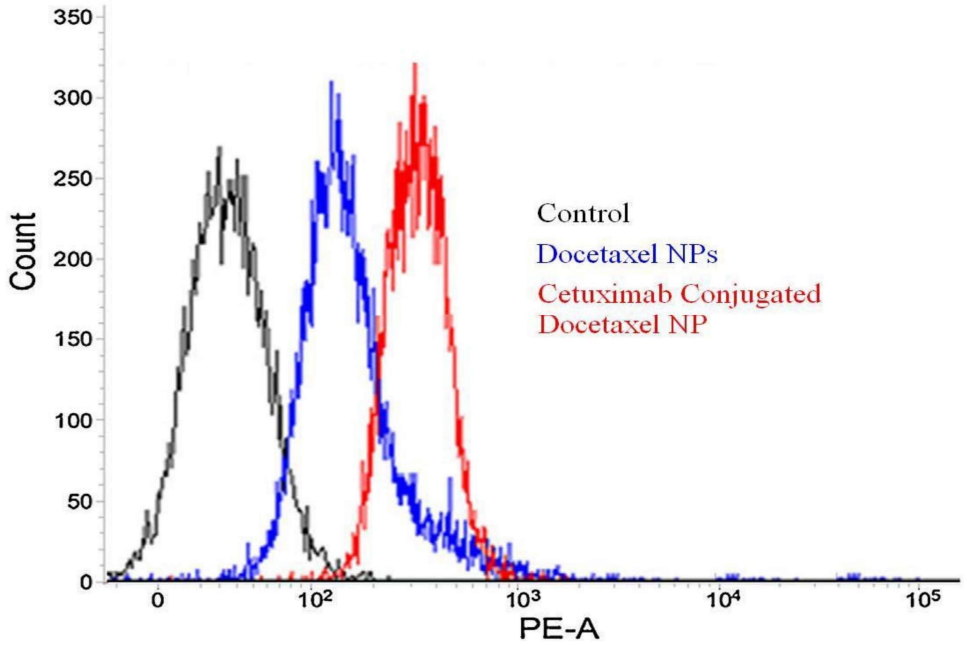

Figure 5.4 Cellular uptake analysis of Cetuximab conjugated Docetaxel nanoparticles in A549 cells using flow cytometer.

5.2.4 Cell apoptosis analysis

Annexin V-FITC staining in conjunction with PI can differentiate early apoptosis and late apoptosis or proportion of living cells. PI, a standard molecular probe used to distinguish viable cells from nonviable cells. Generally, viable cells having intact membranes do not interact with PI, while membranes of dead cells are permeable to PI. Therefore, annexin V-FITC/ PI staining can distinguish early apoptosis from late apoptosis in cell populations. As a representative, A549 was used to study the apoptotic behavior of formulations. After 24 h incubation, Docetaxel Nanoparticles showed slight apoptosis with majority of cells in the lower right quadrant in the viable cells chamber indicating a moderate DNA fragmentation (8,9,38).

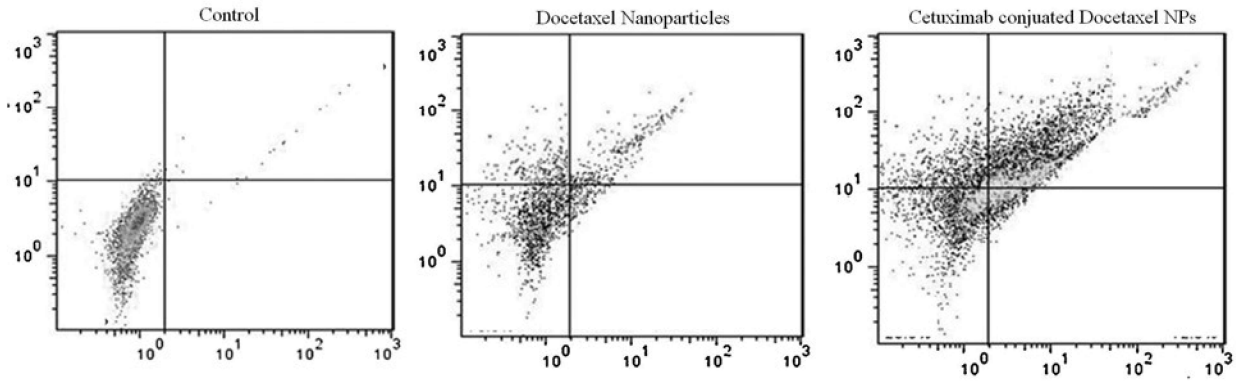

Figure 5.5 Apoptosis analysis of A549 cells after treatment with Docetaxel nanoparticles and Cetuximab conjugated Docetaxel nanoparticles upon 24 h incubation.

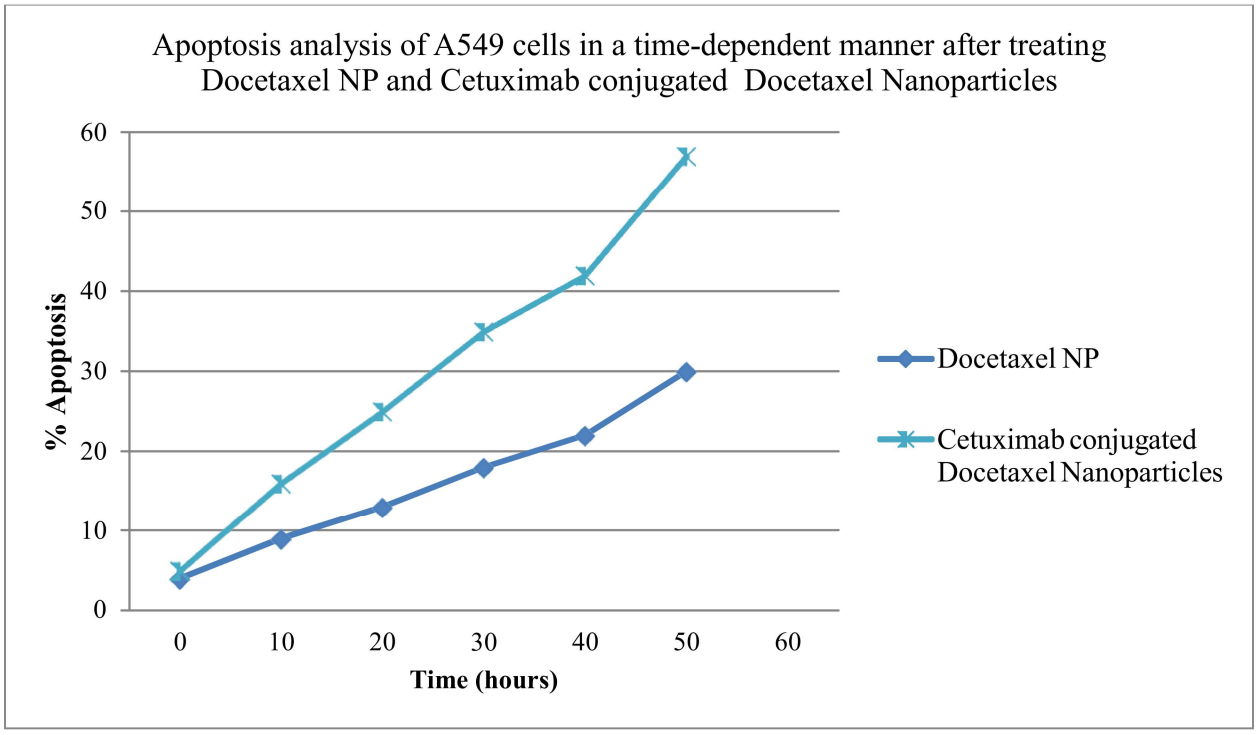

Figure 5.6 Apoptosis analysis of A549 cells in a time-dependent manner after treating Docetaxel NP and Cetuximab conjugated Docetaxel Nanoparticles.

(*$p < 0.05$, **$p < 0.01$, statistical difference between Cetuximab conjugated Docetaxel Nanoparticles and Docetaxel NP)

Cetuximab conjugated Docetaxel Nanoparticles on the other hand markedly induced the apoptosis with predominant amount of cells in the early and late apoptosis stages indicating a strong DNA fragmentation and chromatin condensation. Furthermore, time-dependent apoptosis

was observed using flow cytometry analysis. As shown in **Figure 5.6**, cell apoptosis gradually increased with the increase in the incubation time of respective NP system. A prominent apoptosis was observed at longer incubation time (24 hours and 36 hours) for both the nanoparticulate system (8,26,38).

The explosion of studies on apoptosis in recent years has described it as a regulated, controlled and complex process of autonomous cellular dismantling, also referred as programmed cell death. Cells undergoing apoptosis show characteristic morphological and biochemical features. These features include chromatin aggregation, nuclear and cytoplasmic condensation. On the contrary, necrosis represents a passive consequence of gross injury to the cell. It is morphologically different from apoptosis, and its physiological consequences are also very different from those of apoptosis (41).

Necrosis begins with an impairment of the cell's ability to maintain homeostasis, leading to an influx of water and extracellular ions. To determine if inhibition of EGFR resulted in apoptosis of A549 cell line, apoptosis studies was conducted using Annexin V staining procedure. Cetuximab conjugated Docetaxel Nanoparticles were able to cause more apoptosis and necrosis in A549 cell lines as compared to drug loaded nanoparticles and native drug following site specific sustained delivery pattern. Additionally it was observed that dose elevation of drug results in reduction of the degree of apoptosis as tumor necrosis increases. In our study, native docetaxel diffuses and accumulates directly at site of action at a higher concentration thus resulting in necrosis. However, nanoparticles show a slow sustained release phenomenon and at a lower dose apoptosis signals may be activated leading to a higher number of cell deaths. On contrary targeted therapy showed mixed results, with cells being present both in apoptosis phase as well as in necrosis stage. Targeted delivery and better uptake of Cetuximab conjugated Docetaxel Nanoparticles results in greater accumulation of drug loaded nanoparticles inside tumor tissue (35). Confocal microscopic images of A549 cells are given as Figure 6. Rapid release of surface adsorbed drug (burst release) from nanoparticles is responsible for causing necrosis initially in the A549 cells. However, in later stages slow and sustained release of drug molecules is responsible for eliciting apoptotic signals causing death by apoptosis.(8,41) Sustained cytoplasmic delivery of the drug from nanoparticles coupled with the site specific delivery of docetaxel due to EGFRs have resulted in more enhanced therapeutic potency of the Cetuximab conjugated Docetaxel Nanoparticles by apoptosis than unconjugated nanoparticles

thus, supporting the idea that surface modified nanoparticle can serve as effective delivery vehicles. As expected, Cetuximab conjugated Docetaxel Nanoparticles exhibited greater apoptotic populations than comparing to Docetaxel Nanoparticles throughout the study period. Therefore it can be expected that Cetuximab effectively bind to Anti EGFR receptor and release the drug to tumourous cells and induced a strong synergism .

5.2.5 Cell cycle analysis

Docetaxel tightly binds with the microtubules and promotes its stabilization resulting in the mitotic arrest of cancer cells. It is well known that Docetaxel induce cell cycle arrest by impairing mitosis and chromosomal damage, thereby induce typical G2/M phase arrest. The polymerization and depolymerization of microtubules has an important role in biological process. The Docetaxel nanoparticles, and Cetuximab conjugated Docetaxel nanoparticles were exposed to A549 and incubated for 15 hours. As can be seen, control cells largely present in G1 phase with around 5% in G2/M phase (**Figure 5.7**).

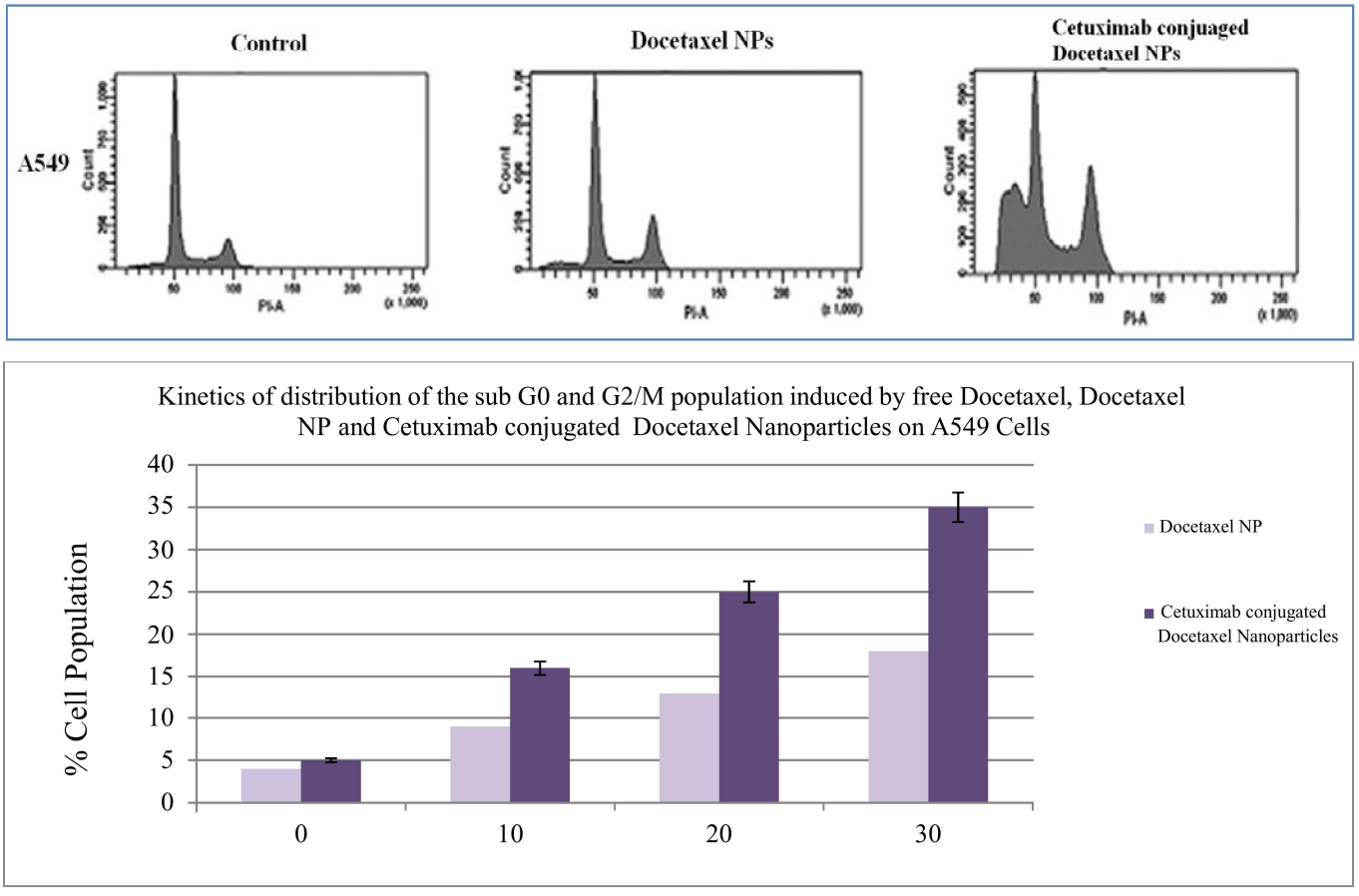

Figure 5.7 Cell cycle distribution in A549 cells using flow cytometry.

The cells were treated with Docetaxel nanoparticles, and Cetuximab conjugated Docetaxel nanoparticles (Docetaxel equivalent concentration 1 mg/ ml). Kinetics of distribution of the sub-G0 and G2/M population induced by Docetaxel nanoparticles, and Cetuximab conjugated Docetaxel nanoparticles in A549 cells (37,38,41).

The treatment with Docetaxel nanoparticulate system however resulted in significant G2/M phase arrest in both the cell lines. Interestingly, Cetuximab conjugated Docetaxel nanoparticles exhibited remarkable increase in sub-G0/G1 phase, indicating increasing hypodiploids or apoptotic cells. A remarkable increase in G2/M phase arrest accompanied with significant proportion of apoptotic cells indicates the synergistic cytotoxic action (**Figure 5.7**).

Cell cycle analysis demonstrated that the cells treated with docetaxel had a higher proportion of cells in the G1 phase. It was observed that a higher proportion of cells were in the G1 arrest phase following treatment by Cetuximab conjugated Docetaxel Nanoparticles and Docetaxel Nanoparticles than the cells treated with the native docetaxel drug. There are previous reports confirming higher arrest of higher number of cells in G0/G1 phase when treated with nanoparticles as compared to free drug treated cells (36). However, Cetuximab conjugated Docetaxel Nanoparticles inhibiting a greater number of cells in G1 phase can be explained based on the intracellular drug levels. It can be said that in case of nanoparticle mediated targeted therapy more drug is available at the site of action (following sustained drug release) for a longer period than native drug in solution, resulting in greater efficiency of the Cetuximab conjugated Docetaxel Nanoparticles in arresting cell growth (34).

It has been reported that docetaxel acts at molecular level by impairing mitosis and inducing cell cycle arrest [40]. **Figure 5.7** depicts the results of treating A549 cells for 24 hours with Docetaxel Nanoparticles and Cetuximab conjugated Docetaxel Nanoparticles at IC50 values. All treatments induced accumulation in G2/M and S phases, with a significant decrease in G0/G1 phase *versus* control cells. The accumulation was significantly greater in cells treated with Cetuximab conjugated Docetaxel Nanoparticles than in cells treated with the Docetaxel Nanoparticles and free Docetaxel (Figure 5.3). The rapid decrease in cell cycle progression, evidenced by the increased percentage of cells in S and G2/M phase, is in agreement with

previous reports that docetaxel treatment induces a G2 cell cycle build up in several cell lines, including A549.(34,38)

Reference List

1. Clift MJD, Rothen-Rutishauser B, Brown DM, Duffin R, Donaldson K, Proudfoot L, et al. The impact of different nanoparticle surface chemistry and size on uptake and toxicity in a murine macrophage cell line. Toxicol Appl Pharmacol [Internet]. 2008;232(3):418–27. Available from: http://www.sciencedirect.com/science/article/pii/S0041008X08002640

2. Faraji AH, Wipf P. Nanoparticles in cellular drug delivery. Bioorganic and Medicinal Chemistry. 2009. p. 2950–62.

3. Liu Y, Peterson DA, Kimura H, Schubert D. Mechanism of cellular 3-(4,5-dimethylthiazol-2-yl)-2,5-diphenyltetrazolium bromide (MTT) reduction. J Neurochem [Internet]. 1997;69(2):581–93. Available from: http://www.ncbi.nlm.nih.gov/pubmed/9231715

4. Romero G, Estrela-Lopis I, Zhou J, Rojas E, Franco A, Espinel CS, et al. Surface engineered poly(lactide-co-glycolide) nanoparticles for intracellular delivery: Uptake and cytotoxicity - A confocal Raman microscopic study. Biomacromolecules. 2010;11(11):2993–9.

5. Stockert JC, Bl??zquez-Castro A, Ca??ete M, Horobin RW, Villanueva ??ngeles. MTT assay for cell viability: Intracellular localization of the formazan product is in lipid droplets. Acta Histochem. 2012;114(8):785–96.

6. Ben Reguiga M, Bouquet C, Farinotti R, Bonhomme-Faivre L. Interferon-alpha improves docetaxel antitumoral and antimetastatic efficiency in Lewis lung carcinoma bearing mice. Life Sci [Internet]. 2012 Oct 29 [cited 2016 Feb 15];91(17-18):843–51. Available from: http://www.sciencedirect.com/science/article/pii/S0024320512004778

7. Esmaeili F, Ghahremani MH, Ostad SN, Atyabi F, Seyedabadi M, Malekshahi MR, et al. Folate-receptor-targeted delivery of docetaxel nanoparticles prepared by PLGA-PEG-folate conjugate. J Drug Target. 2008;16(5):415–23.

8. Jain A, Thakur K, Kush P, Jain UK. Docetaxel loaded chitosan nanoparticles: formulation, characterization and cytotoxicity studies. Int J Biol Macromol [Internet]. 2014 Aug [cited

2016 Feb 15];69:546–53. Available from: http://www.sciencedirect.com/science/article/pii/S0141813014004127

9. Jain A, Thakur K, Sharma G, Kush P, Jain UK. Fabrication, characterization and cytotoxicity studies of ionically cross-linked docetaxel loaded chitosan nanoparticles. Carbohydr Polym [Internet]. 2016 Feb [cited 2015 Nov 18];137:65–74. Available from: http://www.sciencedirect.com/science/article/pii/S0144861715009923

10. Maddox PS. Confocal imaging of cell division. Curr Protoc Cytom [Internet]. 2008;Chapter 12(January):Unit12.11. Available from: http://www.ncbi.nlm.nih.gov/pubmed/18770643

11. Pawley JB. Limitations on optical sectioning in live-cell confocal microscopy. Scanning [Internet]. 2002;24(5):241–6. Available from: http://www.ncbi.nlm.nih.gov/pubmed/12392355

12. Pygall SR, Whetstone J, Timmins P, Melia CD. Pharmaceutical applications of confocal laser scanning microscopy: The physical characterisation of pharmaceutical systems. Advanced Drug Delivery Reviews. 2007. p. 1434–52.

13. Stelzer EH, Wacker I, De Mey JR. Confocal fluorescence microscopy in modern cell biology. Semin Cell Biol. 1991;2:145–52.

14. Wright SJ, Wright DJ. Introduction to confocal microscopy. [Internet]. Methods in cell biology. 2002. 1-85 p. Available from: http://dx.doi.org/10.1016/S0091-679X(02)70002-2

15. Földes-Papp Z, Demel U, Tilz GP. Laser scanning confocal fluorescence microscopy: An overview. International Immunopharmacology. 2003. p. 1715–29.

16. Wang T, Bai J, Jiang X, Nienhaus GU. Cellular uptake of nanoparticles by membrane penetration: A study combining confocal microscopy with FTIR spectroelectrochemistry. ACS Nano. 2012;6(2):1251–9.

17. Dailey ME, Manders E, Soll DR, Terasaki M. Confocal Microscopy of Living Cells. Methods. 2006;381–404.

18. Ducat E, Evrard B, Peulen O, Piel G. Cellular uptake of liposomes monitored by confocal microscopy and flow cytometry. J Drug Deliv Sci Technol [Internet]. 2011 [cited 2016 Feb 13];21(6):469–77. Available from: http://www.sciencedirect.com/science/article/pii/S1773224711500760

19. Klein S, Petersen S, Taylor U, Rath D, Barcikowski S. Quantitative visualization of colloidal and intracellular gold nanoparticles by confocal microscopy. J Biomed Opt. 2013;15(3):036015.

20. Kutty RV, Feng S-S. Cetuximab conjugated vitamin E TPGS micelles for targeted delivery of docetaxel for treatment of triple negative breast cancers. Biomaterials [Internet]. 2013 Dec [cited 2016 Feb 15];34(38):10160–71. Available from: http://www.sciencedirect.com/science/article/pii/S0142961213011265

21. Paddock SW. Principles and practices of laser scanning confocal microscopy. Mol Biotechnol. 2000;16(2):127–49.

22. Paddock SW. Confocal laser scanning microscopy. BioTechniques. 1999. p. 992–1004.

23. Yameen B, Choi W Il, Vilos C, Swami A, Shi J, Farokhzad OC. Insight into nanoparticle cellular uptake and intracellular targeting. J Control Release [Internet]. 2014 Sep [cited 2015 Oct 14];190:485–99. Available from: http://www.sciencedirect.com/science/article/pii/S0168365914004477

24. Portis AM, Carballo G, Baker GL, Chan C, Walton SP. Confocal microscopy for the analysis of siRNA delivery by polymeric nanoparticles. Microsc Res Tech. 2010;73(9):878–85.

25. Zinchuk V, Grossenbacher-Zinchuk O. Quantitative colocalization analysis of confocal fluorescence microscopy images. Curr Protoc Cell Biol. 2011;(SUPPL. 52).

26. Qaddoumi MG, Ueda H, Yang J, Davda J, Labhasetwar V, Lee VHL. The characteristics and mechanisms of uptake of PLGA nanoparticles in rabbit conjunctival epithelial cell layers. Pharm Res. 2004;21(4):641–8.

27. Tahara K, Sakai T, Yamamoto H, Takeuchi H, Hirashima N, Kawashima Y. Improved cellular uptake of chitosan-modified PLGA nanospheres by A549 cells. Int J Pharm [Internet]. 2009 Dec 1 [cited 2016 Feb 13];382(1-2):198–204. Available from: http://www.sciencedirect.com/science/article/pii/S0378517309004955

28. Tantra R, Knight A. Cellular uptake and intracellular fate of engineered nanoparticles: A review on the application of imaging techniques. Nanotoxicology [Internet]. 2010;1–12. Available from: http://www.ncbi.nlm.nih.gov/pubmed/20846020

29. Cartiera MS, Johnson KM, Rajendran V, Caplan MJ, Saltzman WM. The uptake and intracellular fate of PLGA nanoparticles in epithelial cells. Biomaterials. 2009;30(14):2790–8.

30. Lorenz MR, Holzapfel V, Musyanovych A, Nothelfer K, Walther P, Frank H, et al. Uptake of functionalized, fluorescent-labeled polymeric particles in different cell lines and stem cells. Biomaterials. 2006;27(14):2820–8.

31. Estrela-Lopis I, Romero G, Rojas E, Moya SE, Donath E. Nanoparticle uptake and their co-localization with cell compartments – a confocal Raman microscopy study at single cell level. J Phys Conf Ser [Internet]. 2011;304:012017. Available from: http://stacks.iop.org/1742-6596/304/i=1/a=012017?key=crossref.2f4e486cf860c9bdf414475ead2a65f4

32. Desai MP, Labhasetwar V, Walter E, Levy RJ, Amidon GL. The mechanism of uptake of biodegradable microparticles in Caco-2 cells is size dependent. Pharm Res. 1997;14(11):1568–73.

33. Jiang L, Zhao X, Zheng C, Li F, Maclean JL, Chen F, et al. The quantitative detection of the uptake and intracellular fate of albumin nanoparticles. RSC Adv [Internet]. 2015;5(44):34956–66. Available from: http://www.scopus.com/inward/record.url?eid=2-s2.0-84928335059&partnerID=tZOtx3y1

34. Kann B, Offerhaus HL, Windbergs M, Otto C. Raman microscopy for cellular investigations--From single cell imaging to drug carrier uptake visualization. Adv Drug

Deliv Rev [Internet]. 2015 Jul 15 [cited 2016 Jan 28];89:71–90. Available from: http://www.sciencedirect.com/science/article/pii/S0169409X15000174

35. Khatri N, Baradia D, Vhora I, Rathi M, Misra A. CRGD grafted liposomes containing inorganic nano-precipitate complexed siRNA for intracellular delivery in cancer cells. J Control Release. 2014;182(1):45–57.

36. Li SD, Huang L. Pharmacokinetics and biodistribution of nanoparticles. In: Molecular Pharmaceutics. 2008. p. 496–504.

37. Nikolova K, Kaloyanova S, Mihaylova N, Stoitsova S, Chausheva S, Vasilev A, et al. New fluorogenic dyes for analysis of cellular processes by flow cytometry and confocal microscopy. J Photochem Photobiol B Biol. 2013;129:125–34.

38. Maya S, Sarmento B, Lakshmanan V-K, Menon D, Seabra V, Jayakumar R. Chitosan cross-linked docetaxel loaded EGF receptor targeted nanoparticles for lung cancer cells. Int J Biol Macromol [Internet]. 2014 Aug [cited 2016 Feb 13];69:532–41. Available from: http://www.sciencedirect.com/science/article/pii/S0141813014003924

39. Jia F, Liu X, Li L, Mallapragada S, Narasimhan B, Wang Q. Multifunctional nanoparticles for targeted delivery of immune activating and cancer therapeutic agents. Journal of Controlled Release. 2013. p. 1020–34.

40. Mo Y, Lim LY. Mechanistic Study of the Uptake of Wheat Germ Agglutinin-Conjugated PLGA Nanoparticles by A549 Cells. J Pharm Sci. 2004;93(1):20–8.

41. Prabaharan M. Chitosan-based nanoparticles for tumor-targeted drug delivery. Int J Biol Macromol [Internet]. 2015 Jan [cited 2016 Jan 16];72:1313–22. Available from: http://www.sciencedirect.com/science/article/pii/S0141813014007326